ISSN 1674-1056
http://cpb.iphy.ac.cn
http://iopscience.iop.org/cpb
中国物理 B
Chinese Physics
中国物理 Chinese Physics B

Electrical spin polarization through spin-momentum locking in topological-insulator nanostructures

Minhao Zhang(张敏昊), Xuefeng Wang(王学锋), Fengqi Song(宋凤麒), Rong Zhang(张荣)

Citation: Chin. Phys. B . 2018, 27(9): 097307. **doi:** 10.1088/1674-1056/27/9/097307

Journal homepage: http://cpb.iphy.ac.cn; http://iopscience.iop.org/cpb

What follows is a list of articles you may be interested in

Quantum oscillations and nontrivial transport in $(Bi_{0.92}In_{0.08})_2Se_3$

Minhao Zhang(张敏昊), Yan Li(李焱), Fengqi Song(宋凤麒), Xuefeng Wang(王学锋), Rong Zhang(张荣)
Chin. Phys. B . 2017, 26(12): 127305. **doi:** 10.1088/1674-1056/26/12/127305

Two-dimensional topological insulators with large bulk energy gap

Z Q Yang(杨中强), Jin-Feng Jia(贾金锋), Dong Qian(钱冬)
Chin. Phys. B . 2016, 25(11): 117312. **doi:** 10.1088/1674-1056/25/11/117312

Length dependence of rectification in organic co-oligomer spin rectifiers

Gui-Chao Hu(胡贵超), Zhao Zhang(张朝), Ying Li(李营), Jun-Feng Ren(任俊峰), Chuan-Kui Wang(王传奎)
Chin. Phys. B . 2016, 25(5): 057308. **doi:** 10.1088/1674-1056/25/5/057308

Effect of interfacial coupling on rectification in organic spin rectifiers

Hu Gui-Chao, Zuo Meng-Ying, Li Ying, Zhang Zhao, Ren Jun-Feng, Wang Chuan-Kui
Chin. Phys. B . 2015, 24(7): 077308. **doi:** 10.1088/1674-1056/24/7/077308

Topological edge states and electronic structures of a 2D topological insulator: Single-bilayer Bi (111)

Gao Chun-Lei, Qian Dong, Liu Can-Hua, Jia Jin-Feng, Liu Feng
Chin. Phys. B . 2013, 22(6): 067304. **doi:** 10.1088/1674-1056/22/6/067304

TOPIC REVIEW — Spin manipulation in solids

Electrical spin polarization through spin–momentum locking in topological-insulator nanostructures*

Minhao Zhang(张敏昊)[1], Xuefeng Wang(王学锋)[1,3,†], Fengqi Song(宋凤麒)[2,3], and Rong Zhang(张荣)[1,3,‡]

[1] Jiangsu Provincial Key Laboratory of Advanced Photonic and Electronic Materials, School of Electronic Science and Engineering, Nanjing University, Nanjing 210093, China

[2] School of Physics, Nanjing University, Nanjing 210093, China

[3] National Laboratory of Solid State Microstructures, Collaborative Innovation Center of Advanced Microstructures, Nanjing University, Nanjing 210093, China

(Received 29 April 2018; revised manuscript received 18 May 2018; published online 28 August 2018)

Recently, spin–momentum-locked topological surface states (SSs) have attracted significant attention in spintronics. Owing to spin–momentum locking, the direction of the spin is locked at right angles with respect to the carrier momentum. In this paper, we briefly review the exotic transport properties induced by topological SSs in topological-insulator (TI) nanostructures, which have larger surface-to-volume ratios than those of bulk TI materials. We discuss the electrical spin generation in TIs and its effect on the transport properties. A current flow can generate a pure in-plane spin polarization on the surface, leading to a current-direction-dependent magnetoresistance in spin valve devices based on TI nanostructures. A relative momentum shift of two coupled topological SSs also generates net spin polarization and induces an in-plane anisotropic negative magnetoresistance. Therefore, the spin–momentum locking can enable the broad tuning of the spin transport properties of topological devices for spintronic applications.

Keywords: spin–momentum locking, electrical spin generation, topological insulators, topological devices, spintronics

PACS: 73.50.Jt, 05.30.Rt **DOI:** 10.1088/1674-1056/27/9/097307

1. Introduction

Similar to ordinary insulators, intrinsic three-dimensional (3D) topological insulators (TIs) have insulating bulk states. As the bulk TI and vacuum belong to different topology classes, metallic states exist on the interface between the bulk and the vacuum, referred to as topological surface states (SSs). Each topological SS consists of an odd number of massless Dirac cones, which is ensured by the Z_2 topological invariant.[1–4] One of the most fascinating properties of the SSs is spin–momentum helical locking. A current flow on the surface of a TI generates an in-plane spin polarization, which makes the TIs a new class of spintronics materials.[5–8]

The first reported 3D TI is the alloy $Bi_{1-x}Sb_x$ ($x = 0.1$), experimentally identified by Hsieh *et al.* using angle-resolved photoemission spectroscopy (ARPES).[9] Approximately linear SSs are observed at the Fermi level, spanning the bulk gap for an odd (five) number of times (Fig. 1(a)). Therefore, the SSs of $Bi_{1-x}Sb_x$ ($x = 0.1$) are topologically protected. However, the band structure is complex with many impurity bands within the bulk gap (Fig. 1(a)), which poses challenges in surface transport studies. This has motivated the search for TIs with simpler band structures. The bulk band inversion has been used in the search to evaluate whether a material is TI.[10] For example, Bi_2Se_3,[11,12] Bi_2Te_3,[12,13] and Sb_2Te_3 belong to a new class of 3D TIs with a single Dirac cone, which is not the case for the isostructural material Sb_2Se_3. Bi_2Se_3 has a large bulk gap of ~ 0.3 eV (Fig. 1(b)), significantly larger than the energy scale of room temperature (26 meV). In addition, the Dirac point (DP) of the topological SS is in the bulk gap with no other impurity bands. These properties make it a preferable platform to study the topological SSs. Figure 1(c) shows the rhombohedral crystal structure of Bi_2Se_3. Five atom layers are indicated in the crystal structure of Bi_2Se_3 (Fig. 1(c)), referred to as quintuple layers (QLs). These QLs are bonded together predominantly by van der Waals interactions. Therefore, we can easily obtain TI nanostructures by mechanical exfoliation along the z-direction using scotch tape.

However, the Fermi level of Bi_2Se_3 is positioned deep in the bulk conduction band, as shown in Fig. 1(b). The DP is located at -0.3 eV, significantly below the Fermi level. Therefore, naturally grown Bi_2Se_3 samples exhibit an n-type behavior and are highly metallic, owing to a large amount of Se vacancies.[11,12] For a dominant surface transport, the Fermi level of a TI should be in the bulk gap with a very small bulk carrier density. Significant efforts have been invested to suppress the bulk carrier density in TIs. By appropriate chemi-

*Project supported by the National Key Basic Research Program of China (Grant Nos. 2014CB921103 and 2017YFA0206304), the National Natural Science Foundation of China (Grant Nos. 61822403, 11874203, U1732159, and U1732273), Fundamental Research Funds for the Central Universities, China (Grant No. 021014380080), and Collaborative Innovation Center of Solid-State Lighting and Energy-Saving Electronics, China.

†Corresponding author. E-mail: xfwang@nju.edu.cn

‡Corresponding author. E-mail: rzhang@nju.edu.cn

© 2018 Chinese Physical Society and IOP Publishing Ltd

cal modifications, the Fermi level could be tuned close to the DP.[12–19] For example, the TI $Bi_{2-x}Sb_xTe_{3-y}Se_y$ (BSTS) is preferable to utilize the novel properties of SSs. A series of special combinations of x and y have been reported to yield a higher resistivity than that of Bi_2Se_3.[16–19] The maximum bulk resistivity of $BiSbTeSe_2$ in our study was larger than 10 Ω·cm.[19]

In the past few years, we made important progress in the area of spin-polarized transport in the TIs, which we believe represents one of the most promising directions in the field of TIs. In this brief review, we select two representative spin-polarized transport phenomena based on the spin–momentum locking of SSs. In Section 2, we review the surface charge transport behavior in TI nanostructures. In Section 3, we discuss novel spin-valve signals based on the spin-polarized current in SSs. In Section 4, we discuss spin-scattering-induced anisotropic magnetoresistance (AMR) focusing on its relation with topological phase transition (TPT). In Section 5, we provide an outlook of the prospects for spin and charge transport in TIs for spintronic applications.

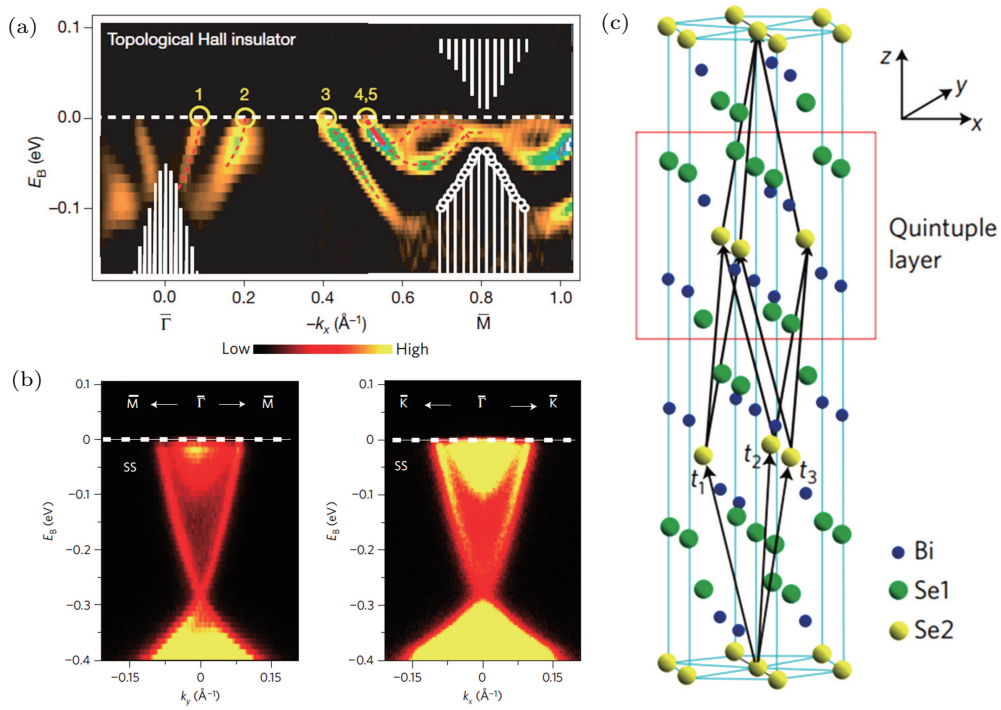


Fig. 1. (color online) (a) Complex band structure of $Bi_{0.9}Sb_{0.1}$ along the $\bar{\Gamma}$–$\bar{M}$ direction.[9] (b) Single Dirac cone of Bi_2Se_3 along the $\bar{\Gamma}$–$\bar{M}$ and $\bar{\Gamma}$–$\bar{K}$ directions.[11] (c) Crystal structure of Bi_2Se_3. A QL is outlined by the red square.[10] This figure is reproduced from Refs. [9]–[11].

2. Surface charge transport behavior in TI nanostructures

In order to study the surface transport behavior of TIs, a low bulk carrier density is not the only requirement. We also need to fabricate TI nanostructures with a higher surface-area-to-volume ratio. The synthesis methods of TI nanostructures include mechanical exfoliation, chemical vapor deposition (CVD), and solvothermal method. Owing to the higher surface-area-to-volume ratios of TI nanowires and nanosheets, the contribution of the SSs to the total magnetoconductance increases. Exotic surface transport behaviors have been demonstrated in nanostructures, such as quantum Hall effect (QHE), quantum oscillations, and weak anti-localization (WAL) effect, which can hardly be observed in bulk samples.

2.1. QHE in TI nanostructures synthesized by mechanical exfoliation

The QHE usually occurs in two-dimensional (2D) systems with low carrier densities at a low temperature and high magnetic field. The bulk part of the sample is insulating, with one-dimensional conducting channels at the edges in the quantum Hall state. QHE originating from SSs has been reported in TI nanostructures[18] obtained by mechanical exfoliation from the corresponding crystals. High-quality TI crystals can be prepared by melting[19–22] or chemical vapor transport[23,24] with a low bulk carrier density and high surface mobility. As the QLs of the TIs are bonded together predominantly by weak van der Waals interactions, the TI nanostructures can be obtained by mechanical exfoliation using scotch tape.

Clear quantization Hall plateaus and vanishing longitudinal conductivity are observed in TI nanostructures. The quantization Hall plateaus are well defined in the units of e^2/h, where e is the electron charge and h is the Planck constant, as the top and bottom SSs always appear as a pair and quantize synchronously.[18,25,26] Each surface Hall conductivity is expected to quantize in units of $(1/2) \times e^2/h$. Therefore, integer quantized Hall plateaus emerge. We also observed integer quantized Hall plateaus (zero and $-e^2/h$) originat-

ing from the SSs at 1.8 K in a high magnetic field of 12 T (Fig. 2(a)).[19] In addition, asynchronous quantization in the conductivity was observed at 1.8 K in a high magnetic field of −7.2 T (Fig. 2(b)). Through the deposition of Co clusters on the top surface of BSTS, we observed a half-integer plateau ($-\frac{3}{2}e^2/h$) (Fig. 2(b)), which demonstrates the quantization trajectory of a single surface. This phenomenon is related to the delayed Landau level. Co clusters on the top surface induce a sizeable Zeeman gap (> 4.8 meV) through antiferromagnetic exchange coupling. Therefore, the Hall quantization of the top surface is delayed, yielding a half-integer plateau ($-\frac{3}{2}e^2/h$) in our bulk-insulating BSTS nanodevices.

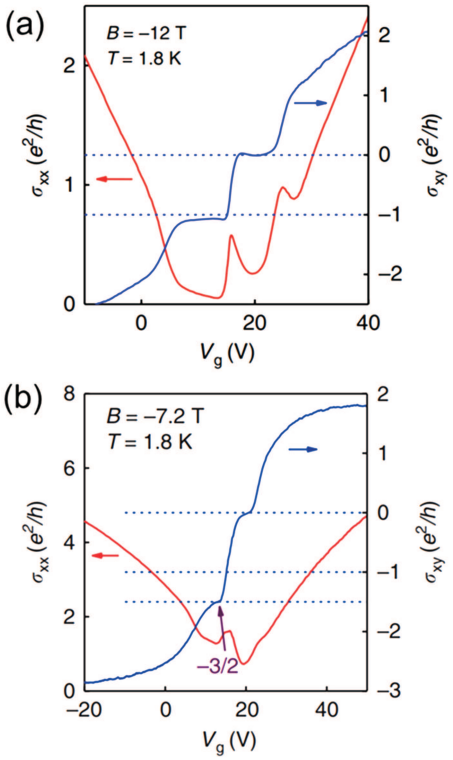


Fig. 2. (color online) QHE of SSs at 1.8 K in a high magnetic field of (a) −12 T and (b) −7.2 T. A half-integer plateau ($-\frac{3}{2}e^2/h$) is observed. This figure is reproduced from Ref. [19].

2.2. Aharonov–Bohm oscillations in TI nanowires fabricated by CVD

High-quality TI nanostructures can be easily grown by the CVD technique. The CVD technique requires a tube furnace equipped with gas flow. One or more precursors are evaporated in a high-temperature region and transported to the substrate for reaction. The growth of TI nanowires is often performed through a vapor–liquid–solid mechanism, which requires catalysts during the crystal growth. The catalysts are often a metal (Au) film or nanoparticles covered on a silicon substrate, helping achieve nucleation of the nanowires.[27–32]

Owing to the π Berry-phase protection, Aharonov–Bohm (AB) oscillations are observed when a magnetic field is applied along the current direction of the TI nanowires. The frequency of the AB oscillations is associated with the cross-section area of the TI nanowires.[33,34] We have grown various types of high-quality topological nanostructures by the CVD technique, including nanoparticles, nanowires, and nanoflowers.[29–32] The good crystallinity of the Bi_2Se_3 nanowires obtained by CVD was verified by high-resolution transmission electron microscopy images. We observed clear AB oscillations in the TI nanowires below 15 K.[29] Figure 3(a) shows the periodic oscillations in a parallel magnetic field at different temperatures below 13 K. We obtained the period of oscillations of $\Delta B \sim 3.01$ T (Fig. 3(b)). Based on the cross-section area of $S \sim 1.56 \times 10^{-15}$ m^2 of the nanowire, we estimate the flux quantum, $\Phi_0 = \Delta B \cdot S \sim h/e$, which is consistent with the AB oscillations. We also observed a peak of $h/2e$ in the inset of Fig. 3(b), attributed to Altshuler–Aronov–Spivak oscillations. The AB oscillations confirm the existence of the topological SSs and coherent surface transport in the TI nanowires.

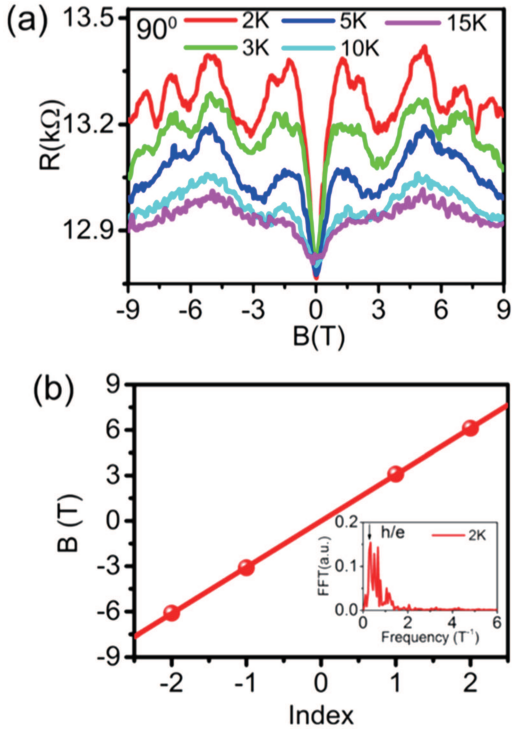


Fig. 3. (color online) (a) AB oscillations at different temperatures. (b) Magnetic-field–oscillation-index plot at 2 K. The inset shows a clear h/e oscillation peak, obtained by fast Fourier transform at 2 K. This figure is reproduced from Ref. [29].

2.3. Well-maintained topological transport of a TI lateral heterojunction obtained by the solvothermal method

TI nanostructures can be grown by the solvothermal method in a solution under high-temperature and high-pressure conditions.[33,35] This also requires a catalyst for nucleation and crystallization. TI nanostructures obtained by the solvothermal method exhibit good qualities, revealed through transport studies. Xiu *et al.* observed clear AB oscillations in Bi_2Te_3 nanoribbons obtained by the solvothermal method.[33] The AB oscillations are regarded as one of the unambiguous

transport evidences of topological SSs. Except TI nanostructures, a lateral TI heterojunction can also be grown by the solvothermal method. We fabricated lateral heterojunctions of Sb_2Te_3/Bi_2Te_3 using a two-step solvothermal method.[36] A sharp boundary was observed in TEM images (inset of Fig. 4(a)), indicating that Sb_2Te_3 and Bi_2Te_3 are well separated. Figure 4(a) shows the magnetoresistance (MR) curve of the heterojunction. A linear MR is clearly observed at high magnetic fields, owing to the linear energy dispersion of the SSs. At low magnetic fields, the MR is parabolic, which can be fitted using Kohler's rule. The fitting results reveal normal values of the carrier mobility and concentration, similar to those of other reported TI nanodevices (Fig. 4(b)). Another signature of topological SSs is the WAL effect in a low magnetic field. A sharp increase in magnetoconductance is observed near zero field in the inset of Fig. 4(a), referred to as the WAL effect. Using the Hikami–Larkin–Nagaoka formula, the fitting for WAL reveals the dephasing length of the SSs, close to those of TI nanostructures without a junction. Therefore, the topological SS is well maintained in our lateral heterojunction obtained by the solvothermal method.

2.4. Transport signature of gapped SSs in TI nanostructures obtained by magnetic doping

Doping in TIs can decrease the number of defects and provide a high resistivity, leading to improved performances of the TIs. We revealed that nonmagnetic Cu doping can enhance the transport contribution of SSs in TIs.[21] In addition, magnetic doping breaks the time-reversal symmetry and induces a gap of SSs. We have grown high-mobility Sm-doped Bi_2Se_3 ferromagnetic TIs, promising for quantum Hall studies.[20] In addition, we have synthesized Fe-doped Bi_2Se_3 nanowires by CVD with a doping concentration of ~ 1 at%.[32] Spontaneous magnetization is induced by Fe doping in Bi_2Se_3 nanowires with a Curie temperature of ~ 40 K. The behavior of the resistance after doping at a low temperature is quite different from that of a pristine sample (Fig. 5(a)). The abnormal behavior

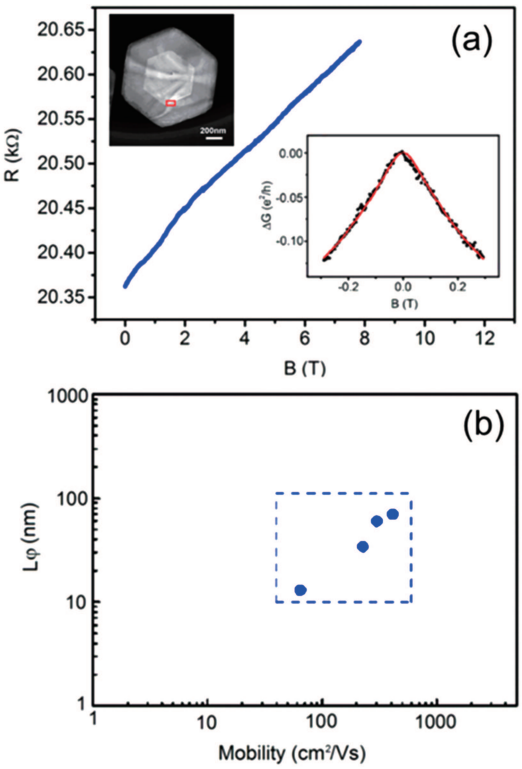


Fig. 4. (color online) (a) MR of the lateral heterojunction device. The left inset shows a TEM image of the lateral heterojunction. The right inset shows the results with the WAL phenomenon and its fitting. (b) Mobility and dephasing length of the lateral heterojunction device. This figure is reproduced from Ref. [36].

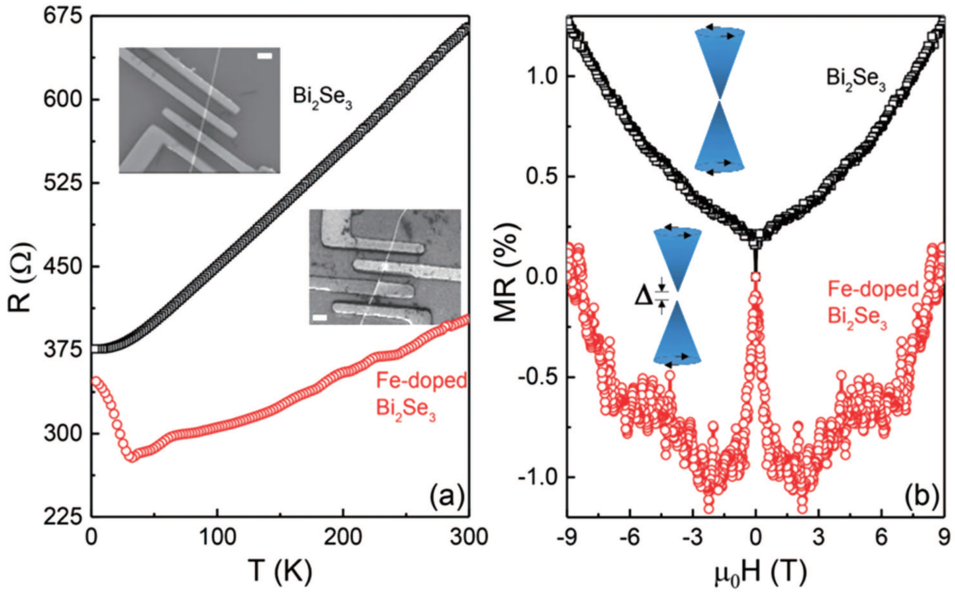


Fig. 5. (color online) (a) Temperature-dependent resistance curves of a pristine and Fe-doped Bi_2Se_3 nanodevices. The insets show scanning-electron-microscopy images of the nanodevices. The scale bars correspond to 1 μm. (b) MRs of the pristine and Fe-doped Bi_2Se_3 nanodevices. A quantum transition from WAL to WL is clearly observed. This figure is reproduced from Ref. [32].

can be attributed to random spin scattering or magnetic impurity scattering upon the Fe doping. The behavior of the MR at a low magnetic field after the doping is also quite different from that of the pristine sample. A quantum transition is observed in Fe-doped TI nanowires, from the WAL to a weak-localization (WL) behavior (Fig. 5(b)).[32] The WL effect was observed in Fe-doped TI nanowires, regarded as a transport signature of the gapped SS. The relationship of the Berry phase (γ) and gap (Δ) can be described as $\gamma = \pi(1 - \Delta/2E_F)$, where E_F is the Fermi level. If there is a gap induced by magnetic scattering, the π Berry phase decreases. Therefore, the WL effect is observed in Fe-doped Bi_2Se_3.

3. Electrical generation of surface spin polarization in TI nanostructures

A spin-based field-effect transistor (SFET) has been proposed in the continuous downscaling of silicon technology. It utilizes the electron spin instead of the charge for a lower power consumption. The discovery of the giant magnetoresistance (GMR) by Albert Fert[37] and Peter Grünberg[38] in 1988 is considered the beginning of the field of spintronics. GMR is observed in films composed of ferromagnetic and nonmagnetic layers.[37–40] Since then, various metals and semiconductors, including Cu,[41] Al,[42] Si,[43,44] Ge,[45,46] GaAs,[47,48] and graphene,[49–51] have been studied for the spin transport channel.

Similar to the conventional charge-based transistors, the SFET consists of a source, drain, channel, and gate for the control of the spin transport.[52–54] The channel is expected to be based on materials with weak spin–orbit couplings, enabling them to transmit spin information with a long spin lifetime and large spin diffusion length. Graphene and Si are of particular interest owing to their unique advantages. Their observed spin lifetimes tend to be approximately several nanoseconds, while the spin diffusion lengths are typically several micrometers at room temperature.[51,55] As important components of the SFET, both source and drain are almost ferromagnets, acting as the injector and detector of an electron spin, respectively. The relative magnetization orientation between them modulates the drivability of the SFET.

However, owing to stray-field effects upon down scaling and integration with the advanced complementary metal-oxide semiconductor technology in the future, all-electric spintronics without ferromagnetic components have attracted increasing attention. Owing to the spin–momentum locking in the TIs, a current flow should induce a spin current on the surface. The direction of the spin polarization is locked at right angles with respect to the current direction. The TIs can realize the all-electrical generation of spin polarization, promising for potential applications in spintronics.

3.1. Detection of spin polarization by spin-resolved ARPES

The spin–momentum-locking property of SSs has been confirmed by optical experiments, including those using spin-resolved ARPES[12,56] and detection of spin-polarized photocurrent.[57,58] Hsieh *et al.* measured the spin polarization of SSs using spin-resolved ARPES.[12] Spin polarization is observed only in the y direction when the momentum is along the x direction. It changes the sign at the opposite momentum, implying that the spin and momentum directions are in-plane locked (Fig. 6(a)). In the x and z directions, no spin polarization can be observed (Fig. 6(b)). Xu *et al.* showed opposite signs of the spin polarizations from electrons and holes (Fig. 6(c)).[56] When the Fermi level is above the DP, the spin vortex is oriented clockwise, whereas the spin vortex of the surface valence band is oriented anticlockwise. Therefore, we can modulate the direction of spin polarization by gating to change the position of the Fermi level through the DP.

3.2. All-electrical generation of spin polarization in TI nanostructures

The electronic spin polarization in the TIs is directly detected using spin-sensitive transport measurements. The spin signal in Bi_2Se_3 has been electrically detected using ferromagnetic contacts.[59–61] Li *et al.* directly measured a novel voltage signal demonstrating the generation of spin polarization in the TIs.[59] The magnitude of the voltage signal is linearly proportional to the magnitude of the charge current. In addition, an opposite voltage signal is observed when the current changes its direction. However, the high bulk conduction in Bi_2Se_3 may be a significant challenge in the detection of the spin polarization. Following this study, several groups used highly insulating bulk TIs or tuned the chemical potential by electrical gating to disentangle the bulk and surface conductions.[62–66] We fabricated spin-valve transistors based on BSTS with an enhanced surface conductance ratio of $\sim 80\%$ (Fig. 7(a)).[66] We observed a dominant step-like spin-valve signal, dependent on the direction of the current (Figs. 7(b) and 7(c)).[66] The conventional spin-valve effect originates from the relative direction of magnetic moments in the ferromagnetic layers and does not depend on the direction of the current. Dankert *et al.* reported generation of spin polarization at room temperature in TIs.[61] The spin polarization can be generated and modulated by charge current, enabling the application of the TIs in spintronics.

Although spin-channel materials with high performances are available, such as graphene and silicon, the use of nonferromagnetic materials as spin injectors is still a major challenge. By utilizing the pure spin-polarized currents generated by a charge current, recently, a TI has been successfully experimentally used to inject spins into a spin-channel material.

Vaklinova *et al.* fabricated a heterostructure device consisting of a TI and graphene (Figs. 8(a) and 8(b)).[67] The TI is used to generate and inject spin into the graphene. They observed a voltage signal originating from the injected spin in graphene (Figs. 8(c) and 8(d)), which exhibits an opposite sign at the opposite current direction. This makes TIs promising spin sources, wherein spin generation is achieved by all-electrical means.

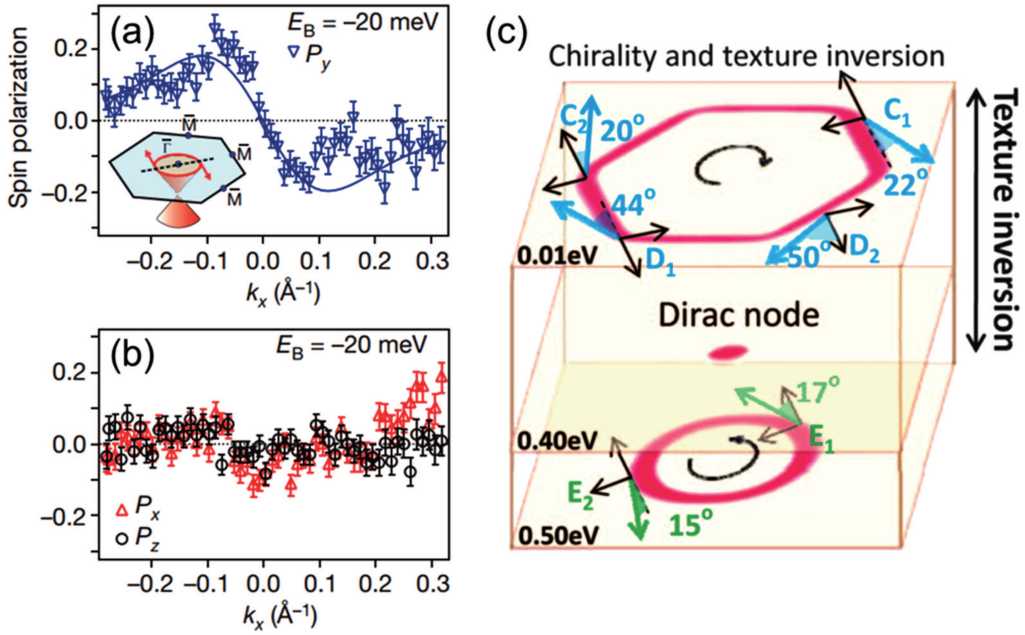


Fig. 6. (color online) Measured (a) *y*, and (b) *x* and *z* components of the spin polarization along the $\bar{\Gamma}$–$\bar{M}$ direction.[12] (c) Spin vortex at the conduction and valence bands.[56] This figure is reproduced from Refs. [12] and [56].

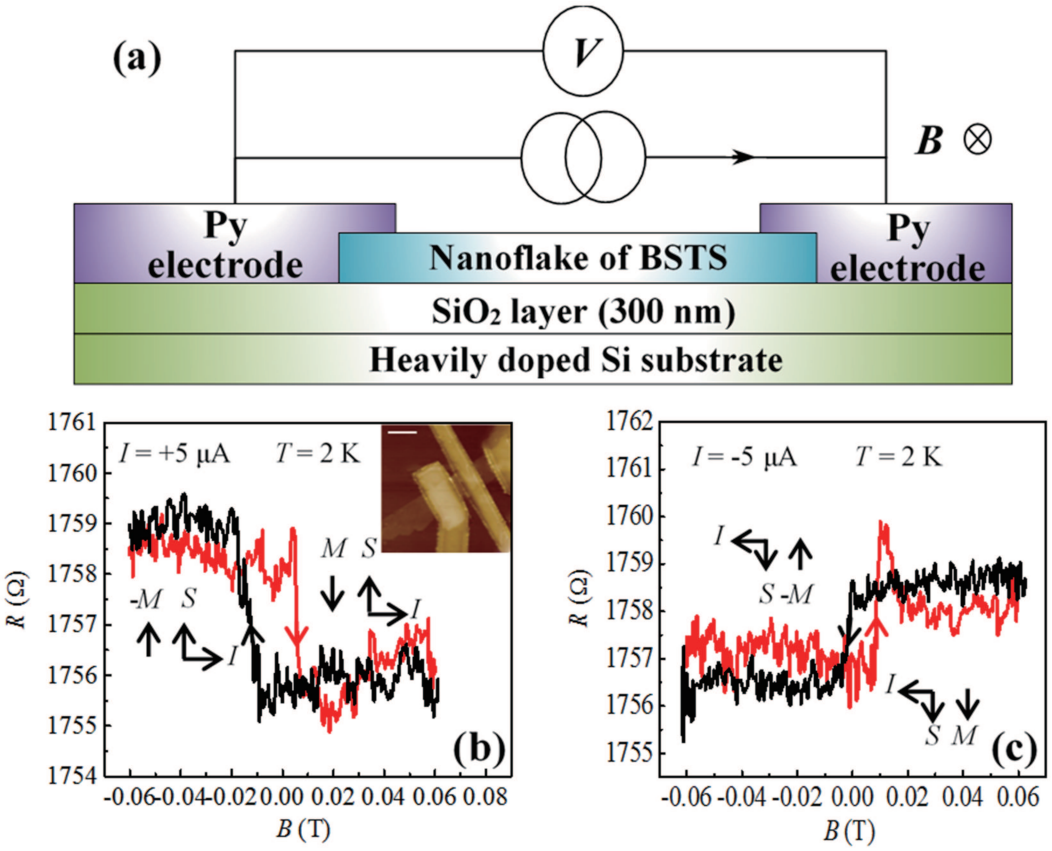


Fig. 7. (color online) (a) Schematic of the spin valve transistors for detection of spin polarization in SSs. (b) and (c) Spin signals under currents of $I_{DC} = +5$ μA and $I_{DC} = -5$ μA, respectively. The inset shows an atomic force microscopy (AFM) image of a spin valve device. The scale bar corresponds to 2.5 μm. This figure is reproduced from Ref. [66].

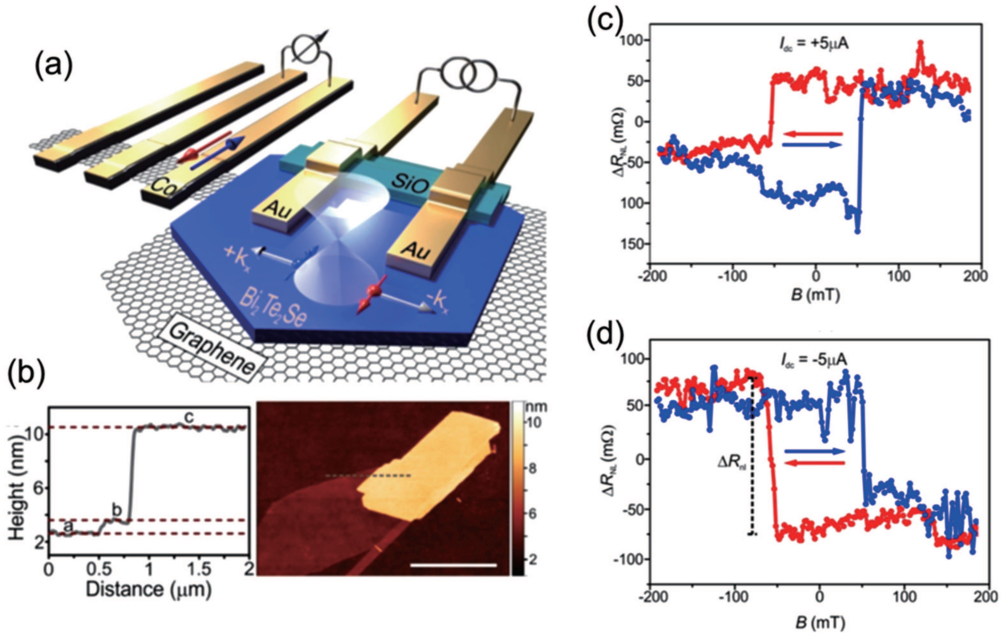


Fig. 8. (color online) (a) Schematic of the heterostructure device. (b) AFM image of a graphene–Bi_2Te_2Se nanoplate heterostructure. (c) and (d) Spin signals in graphene recorded at currents of $I_{dc} = +5$ μA and -5 μA, respectively. This figure is reproduced from Ref. [67].

4. AMR in TI nanostructures

4.1. In-plane AMR in TI nanostructures

The AMR is dependent on the angle between the magnetic field and current in some materials, such as ferromagnetic metals (FMs).[68,69] AMR in FMs is induced by spin-dependent scattering anisotropy, which depends on the relative direction between the current and magnetic moments. In addition, AMR is observed in nonmagnetic materials with strong anisotropies of the mobility and effective mass at the Fermi surface. TIs are a special class of nonmagnetic materials that can generate net spin polarization by current flow. On the other hand, spin polarization emerges in the TI nanostructures when the two SSs couple together in an in-plane magnetic field. The in-plane magnetic field induces a relative momentum shift between the top and bottom SSs. Such net spin polarization induced by an opposite momentum shift is similar to the Rashba splitting in 2D electronic systems.[70] The direction of the spin polarization is along the magnetic field. Moreover, the value of the net spin polarization is proportional to the magnetic field. Therefore, there is a strong anisotropic spin scattering probability dependent on the relative direction between the current and in-plane spin polarization.

Sulaev *et al.* observed an in-plane AMR with a period of 180° in BSTS nanodevices when the two SSs couple together (Fig. 9(a)). The amplitude of the AMR (9 T) reaches 9% at 2 K at a positive gate voltage, comparable with those of some FM metals.[68] They observed an opposite behavior of the AMR at a negative gate voltage (Fig. 9(b)).[71] This AMR is attributed to the high anisotropic spin scattering probability dependent on the relative direction between the current and in-plane spin polarization. The direction of the spin polarization is dependent on the position of the Fermi level.[56] Under a gate voltage of -50 V, the Fermi level is located at the valence band, whereas under a voltage of $+50$ V, the Fermi level is located at the conduction band. The direction of the net spin polarization at the conduction band (Fig. 9(c)) is opposite to that at the valence band at the same magnetic field (Fig. 9(d)), leading to an opposite AMR.

4.2. Enhanced intersurface coupling through TPT and triaxial vector MR devices

It is worth noting that the coupling of the two SSs is the key factor for the in-plane AMR. The top and bottom surfaces can directly couple when the sample is thinner than the critical thickness of ~ 6 nm, which is associated with the bulk gap (0.3 eV). The coupling can also occur in thicker samples through side surfaces or the bulk state in the WAL effect.[72–84] We studied the thickness dependence of bulk-surface coupling in Bi_2Te_2Se nanoribbons.[84] We fitted the number of coherent channels (α) in the nanoribbons from the MR at low magnetic fields. It changes abruptly when the thickness of the nanoribbon exceeds the bulk phase relaxation length of ~ 60 nm (Fig. 10). The bulk carriers are unable to coherently couple the two surfaces when the thickness exceeds the phase relaxation length. The thickness-dependent coherent channels demonstrate bulk-mediated coupling between the top and bottom surfaces. The coupling will not occur when the thickness is significantly larger than the phase relaxation length.

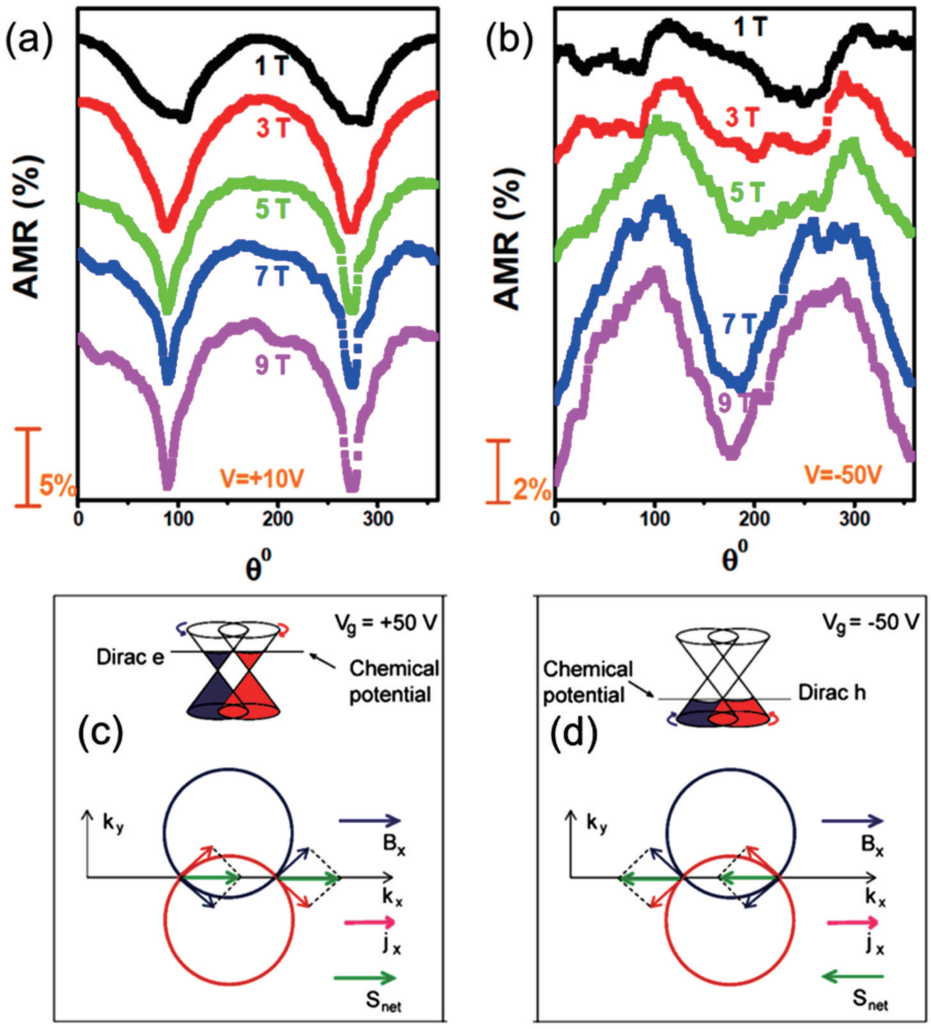


Fig. 9. (color online) (a) and (b) In-plane AMRs under gate voltages of +10 V and −50 V, respectively. (c) and (d) Schematics of the opposite spin polarizations in an in-plane magnetic field under the voltages of +50 V and −50 V, respectively. This figure is reproduced from Ref. [71].

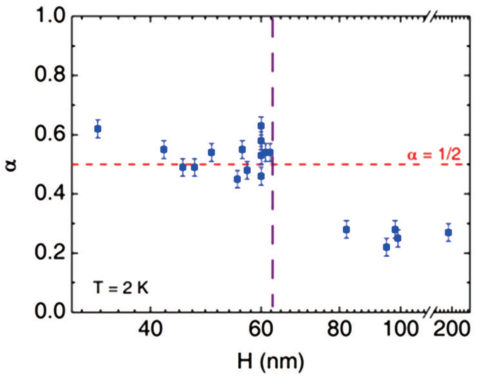


Fig. 10. (color online) Coherent channels (α) as a function of the thickness (H) of different samples. The horizontal dashed line corresponds to one channel. The vertical dashed line corresponds to a phase relaxation length of 62 nm. This figure is reproduced from Ref. [84].

The critical thickness for direct coupling is small ($\sim$ 6 nm) owing to the large bulk gap. The penetration depth of the SS wave function is proportional to $\hbar v_{\mathrm{F}}/\Delta$; therefore, it is small for a large bulk gap, where $\hbar$ is the reduced Planck constant, v_{F} is the Fermi velocity, and Δ is the bulk gap.[85–87] For a close Δ, the threshold for the overlap of the wave functions becomes lower. Therefore, the intersurface coupling could be enhanced by closing the bulk gap Δ near the topological critical point. The TPT in a TI could be employed for artificial engineering of the topological band structure. The TPT of a TI can modulate the band structure of the bulk and surface states and decrease the bulk gap near the topological critical point.[56,88–92]

We studied the TPT by both ARPES and transport measurements in $(Bi_{1-x}In_x)_2Se_3$.[93] $(Bi_{0.92}In_{0.08})_2Se_3$ approaches the topological critical point with the smallest bulk gap ($\sim$ 0.1 eV) among the three series (Fig. 11(a)). Owing to the considerable shrinkage of the bulk gap, the intersurface coupling could be enhanced compared with that of Bi_2Se_3. We measured the angle-dependent MR of $(Bi_{0.92}In_{0.08})_2Se_3$ nanodevices in 3D space (Fig. 11(b)). A negative MR is clearly observed with a high angular sensitivity in the out-of-plane magnetotransport measurements (Fig. 11(c)). A suppressed MR signal is observed with a slight rotation of the magnetic field. Upon further rotation of the magnetic field at the sample

surface, the negative MR is enhanced from $\varphi = 90°$ to $\varphi = 0°$. The negative MR exhibits a period of 180° with an intriguing dumbbell-shaped pattern in its polar diagram (Fig. 11(d)). This novel triaxial MR is observed only in samples with thicknesses in the range of $\sim$ 40–90 nm. The wave functions of the surfaces are strongly coupled in $(Bi_{0.92}In_{0.08})_2Se_3$ (Fig. 11(e)), which will induce spin polarization in the in-plane magnetic field. Owing to the aligned spins along the in-plane magnetic field, the electron scattering is expected to be suppressed, thus driving the negative MR. The in-plane AMR could be interpreted by the angle-dependent scattering probability and still observed at room temperature.

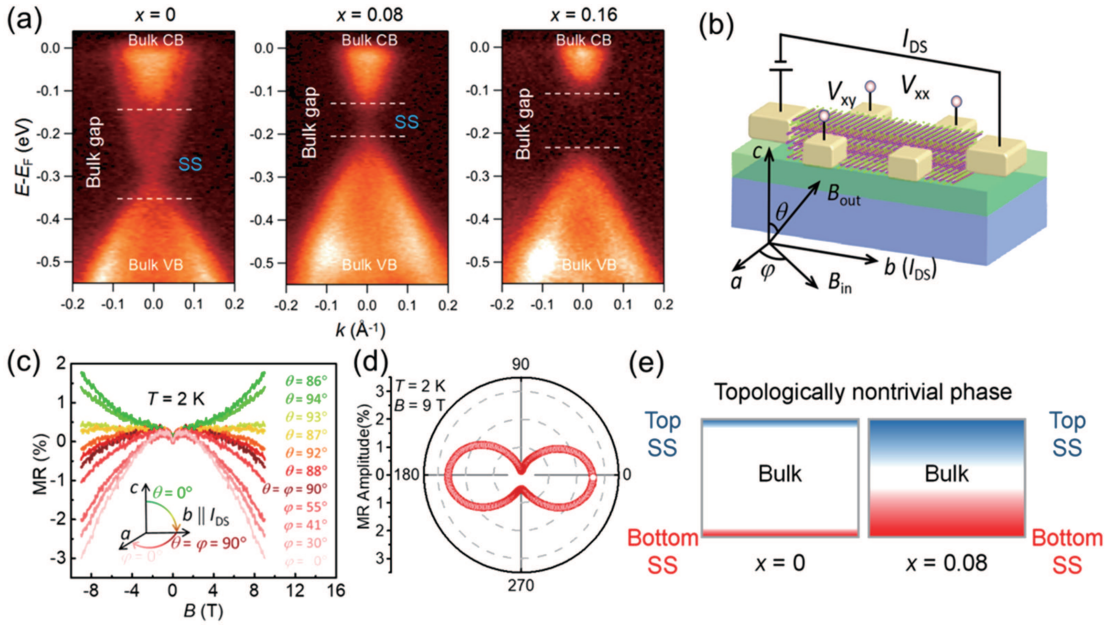


Fig. 11. (color online) (color(a) TPT in the $(Bi_{1-x}In_x)_2Se_3$ series. (b) Schematic of MR measurements of a nanodevice. (c) Triaxial MR curve at 2 K. (d) Polar plot of the AMR. (e) Penetration depth of SS wave functions at $x = 0$ and 0.08. This figure is reproduced from Ref. [93].

5. Conclusion and perspectives

In the period of almost ten years after a 3D TI was successfully observed in 2009, significant progress in spin-polarized transport in TI nanostructures was made. In the preceding sections, we discussed the effects of the net spin polarization on the transport properties, including current-direction-dependent MR and triaxial AMR signals. This suggests the potential for applications in electrical-controlled nonvolatile spintronics and logic devices with significantly enhanced energy efficiencies.

Progress has been made utilizing homoepitaxial tunnel-barrier contacts to achieve an efficient spin injection. Yang *et al.* revealed that the tunneling conductance exhibits the barrier-dependent conductive switching effect with the increase of the barrier strength.[94] Significant achievements have been also made in other areas such as spin transfer torque[95–98] and spin pumping[99–102] in the TIs. Despite these achievements, there are various challenges to overcome in order to realize the SFET based on the TIs. The TI nanostructures are preferable to decrease the bulk state contribution owing to the larger surface-to-volume ratios. This provides an ideal platform to investigate the exotic properties induced by the topological SSs. We expect that optimization of the material growth techniques as well as utilization of the gate tunability and band engineering can enable these properties of TIs (such as AMR and electrical spin generation) to be utilized for future spintronic applications. The continuous development of TIs for spin injection paves the way for novel spintronic device designs for energy-efficient SFET applications.

References

[1] Fu L, Kane C L and Mele E J 2007 *Phys. Rev. Lett.* **98** 106803
[2] Moore J E and Balents L 2007 *Phys. Rev. B* **75** 121306
[3] Hasan M Z and Kane C L 2010 *Rev. Mod. Phys.* **82** 3045
[4] Qi X L and Zhang S C 2011 *Rev. Mod. Phys.* **83** 1057
[5] Burkov A A and Hawthorn D G 2010 *Phys. Rev. Lett.* **105** 066802
[6] Culcer D, Hwang E H, Stanescu T D and Sarma S D 2010 *Phys. Rev. B* **82** 155457
[7] Yazyev O, Moore J and Louie S 2010 *Phys. Rev. Lett.* **105** 266806
[8] Li X and Yang J 2016 *Natl. Sci. Rev.* **3** 365
[9] Hsieh D, Qian D, Wray L, Xia Y, Hor Y S, Cava R J and Hasan M Z 2008 *Nature* **452** 970
[10] Zhang H, Liu C X, Qi X L, Dai X, Fang Z and Zhang S C 2009 *Nat. Phys.* **5** 438
[11] Xia Y, Qian D, Hsieh D, Wray L, Pal A, Lin H, Bansil A, Grauer D, Hor Y S, Cava R J and Hasan M Z 2009 *Nat. Phys.* **5** 398
[12] Hsieh D, Xia Y, Qian D, Wray L, Dil J H, Meier F, Osterwalder J, Patthey L, Checkelsky J G, Ong N P, Fedorov A V, Lin H, Bansil A, Grauer D, Hor Y S, Cava R J and Hasan M Z 2009 *Nature* **460** 1101
[13] Chen Y L, Analytis J G, Chu J H, Liu Z K, Mo S K, Qi X L, Zhang H J, Lu D H, Dai X, Fang Z, Zhang S C, Fisher I R, Hussain Z and Shen Z X 2009 *Science* **325** 178
[14] Ren Z, Taskin A A, Sasaki S, Segawa K and Ando Y 2010 *Phys. Rev. B* **82** 241306
[15] Xiong J, Petersen A C, Qu D X, Hor Y S, Cava R J and Ong N P 2012 *Physica E* **44** 917

[16] Arakane T, Sato T, Souma S, Kosaka K, Nakayama K, Komatsu M, Takahashi T, Zhi R, Segawa K and Ando Y 2012 *Nat. Commun.* **3** 636
[17] Xia B, Ren P, Sulaev A, Liu P, Shen S Q and Wang L 2013 *Phys. Rev. B* **87** 085442
[18] Xu Y, Miotkowski I, Liu C, Tian J, Nam H, Alidoust N, Hu J, Shih C K, Hasan M Z and Chen Y P 2014 *Nat. Phys.* **10** 956
[19] Zhang S, Pi L, Wang R, Yu G, Pan X C, Wei Z, Zhang J, Xi C, Bai Z, Fei F, Wang M, Liao J, Li Y, Wang X, Song F, Zhang Y, Wang B, Xing D and Wang G 2017 *Nat. Commun.* **8** 977
[20] Chen T, Liu W, Zheng F, Gao M, Pan X, Van d L G, Wang X, Zhang Q, Song F, Wang B, Wang B, Xu Y, Wang G and Zhang R 2015 *Adv. Mater.* **27** 4823
[21] Chen T, Chen Q, Schouteden K, Huang W, Wang X, Li Z, Miao F, Wang X, Li Z, Zhao B, Li S, Song F, Wang J, Wang B, Van Haesendonck C and Wang G 2014 *Nat. Commun.* **5** 5022
[22] Zhang M, Li Y, Song F, Wang X and Zhang R 2017 *Chin. Phys. B* **26** 127305
[23] Wang X, Pan X, Gao M, Yu J, Jiang J, Zhang J, Zuo H, Zhang M, Wei Z, Niu W, Xia Z, Wan X, Chen Y, Song F, Xu Y, Wang B, Wang G and Zhang R 2016 *Adv. Electron. Mater.* **2** 1600228
[24] Pan X C, Chen X, Liu H, Feng Y, Wei Z, Zhou Y, Chi Z, Pi L, Yen F, Song F, Wan X, Yang Z, Wang B, Wang G and Zhang Y 2015 *Nat. Commun.* **6** 7805
[25] Nielsen H B and Ninomiya M 1981 *Phys. Lett. B* **105** 219
[26] Yoshimi R, Tsukazaki A, Kozuka Y, Falson J, Takahashi K S, Checkelsky J G, Nagaosa N, Kawasaki M and Tokura Y 2015 *Nat. Commun.* **6** 6627
[27] Yan Y, Liao Z M, Zhou Y B, Wu H C, Bie Y Q, Chen J J, Meng J, Wu X S and Yu D P 2013 *Sci. Rep.* **3** 1264
[28] Kong D, Randel J C, Peng H, Cha J J, Meister S, Lai K, Chen Y, Shen Z X, Manoharan H C and Cui Y 2010 *Nano Lett.* **10** 329
[29] Pan H, Zhang K, Wei Z, Wang J, Han M, Song F, Wang X, Wang B and Zhang R 2017 *Appl. Phys. Lett.* **110** 053108
[30] Zhang K, Pan H, Wei Z, Zhang M, Song F, Wang X and Zhang R 2017 *Chin. Phys. B* **26** 324
[31] Zhang K, Pan H, Zhang M, Wei Z, Gao M, Song F, Wang X and Zhang R 2017 *Rsc Adv.* **7** 17689
[32] Niu W, Du K, Wang S, Zhang M, Gao M, Chen Y, Liu H, Zhou W, Song F, Wang P, Xu Y, Wang X, Shen J and Zhang R 2017 *Nanoscale* **9** 12372
[33] Xiu F, He L, Wang Y, Cheng L, Chang L T, Lang M, Huang G, Kou X, Zhou Y, Jiang X, Chen Z, Zou J, Shailos A and Wang K 2011 *Nat. Nanotech.* **6** 216
[34] Jauregui L A, Pettes M T, Rokhinson L P, Shi L and Chen Y P 2016 *Nat. Nanotech.* **11** 345
[35] Kong D, Koski K J, Cha J J, Hong S S and Cui Y 2013 *Nano Lett.* **13** 632
[36] Fei F, Wei Z, Wang Q J, Lu P, Wang S, Qin Y, Pan D, Zhao B, Wang X, Sun J, Wang X, Wang P, Wan J, Zhou J, Han M, Song F, Wang B and Wang G 2015 *Nano Lett.* **15** 5905
[37] Baibich M N, Broto J M, Fert A, Van Dau F N, Petroff F, Etienne P, Creuzet G, Friederich A and Chazelas J 1988 *Phys. Rev. Lett.* **61** 2472
[38] Barnaś J, Fuss A, Camley R, Grünberg P and Zinn W 1990 *Phys. Rev. B* **42** 8110
[39] Zhou Y, Yang C S, Yu J Q, Zhao X L and Mao H P 2000 *Chin. Phys. Lett.* **17** 835
[40] Huang L, Liu L, Wang R and Hu L 2017 *Chin. Phys. B* **26** 077201
[41] Jedema F J, Filip A and Van Wees B 2001 *Nature* **410** 345
[42] Jedema F, Heersche H, Filip A, Baselmans J and Van Wees B 2002 *Nature* **416** 713
[43] Jonker B T, Kioseoglou G, Hanbicki A T, Li C H and Thompson P E 2007 *Nat. Phys.* **3** 542
[44] Dash S P, Sharma S, Patel R S, de Jong M P and Jansen R 2009 *Nature* **462** 491
[45] Zhou Y, Han W, Chang L T, Xiu F, Wang M, Oehme M, Fischer I A, Schulze J, Kawakami R K and Wang K L 2011 *Phys. Rev. B* **84** 125323
[46] Jeon K R, Min B C, Jo Y H, Lee H S, Shin I J, Park C Y, Park S Y and Shin S C 2011 *Phys. Rev. B* **84** 165315
[47] Lou X, Adelmann C, Crooker S A, Garlid E S, Zhang J, Reddy K M, Flexner S D, Palmstrøm C J and Crowell P A 2007 *Nat. Phys.* **3** 197
[48] Zhu H, Ramsteiner M, Kostial H, Wassermeier M, Schönherr H P and Ploog K 2001 *Phys. Rev. Lett.* **87** 016601
[49] Tombros N, Jozsa C, Popinciuc M, Jonkman H T and Van Wees B J 2007 *Nature* **448** 571
[50] Han W, Pi K, McCreary K, Li Y, Wong J J, Swartz A and Kawakami R 2010 *Phys. Rev. Lett.* **105** 167202
[51] Kamalakar M V, Groenveld C, Dankert A and Dash S P 2015 *Nat. Commun.* **6** 6766
[52] Datta S and Das B 1990 *Appl. Phys. Lett.* **56** 665
[53] Johnson M 1993 *Science* **260** 320
[54] Sugahara S and Tanaka M 2004 *Appl. Phys. Lett.* **84** 2307
[55] Sasaki T, Ando Y, Kameno M, Tahara T, Koike H, Oikawa T, Suzuki T and Shiraishi M 2014 *Phys. Rev. Appl.* **2** 034005
[56] Xu S Y, Xia Y, Wray L A, Jia S, Meier F, Dil J H, Osterwalder J, Slomski B, Bansil A, Lin H, Cava R J and Hasan M Z 2011 *Science* **332** 560
[57] Mciver J W, Hsieh D, Steinberg H, Jarillo Herrero P and Gedik N 2012 *Nat. Nanotech.* **7** 96
[58] Park C H and Louie S G 2012 *Phys. Rev. Lett.* **109** 097601
[59] Li C, van't Erve O, Robinson J, Liu Y, Li L and Jonker B 2014 *Nat. Nanotech.* **9** 218
[60] Tian J, Childres I, Cao H, Shen T, Miotkowski I and Chen Y P 2014 *Solid State Commun.* **191** 1
[61] André D, Johannes G, M Venkata K, Sophie C and Dash S P 2015 *Nano Lett.* **15** 7976
[62] Ando Y, Hamasaki T, Kurokawa T, Ichiba K, Yang F, Novak M, Sasaki S, Segawa K, Ando Y and Shiraishi M 2014 *Nano Lett.* **14** 6226
[63] Tang J, Chang L T, Kou X, Murata K, Choi E S, Lang M, Fan Y, Jiang Y, Montazeri M, Jiang W, Wang Y, He L and Wang K 2014 *Nano Lett.* **14** 5423
[64] Lee J S, Richardella A, Hickey D R, Mkhoyan K A and Samarth N 2015 *Phys. Rev. B* **92** 155312
[65] Tian J, Miotkowski I, Hong S and Chen Y P 2015 *Sci. Rep.* **5** 14293
[66] Zhang M, Wang X, Zhang S, Gao Y, Yu Z, Zhang X, Gao M, Song F, Du J, Wang X, He L, Xu Y and Zhang R 2016 *IEEE Electron. Dev. Lett.* **37** 1231
[67] Vaklinova K, Hoyer A, Burghard M and Kern K 2016 *Nano Lett.* **16** 2595
[68] Zhao C J, Ding L, Huangfu J S, Zhang J Y and Yu G H 2013 *Rare Met.* **32** 213
[69] Xu Y and Cai J W 2011 *Acta Phys. Sin.* **60** 117308 (in Chinese)
[70] Xiong J W, Hu L B and Zhang Z X 2006 *Chin. Phys. Lett.* **23** 1278
[71] Sulaev A, Zeng M, Shen S Q, Cho S K, Wei G Z, Yuan P F, Eremeev S V, Kawazoe Y, Lei S and Lan W 2015 *Nano Lett.* **15** 2061
[72] Cha J J, Claassen M, Kong D, Hong S S, Koski K J, Qi X L and Yi C 2012 *Nano Lett.* **12** 4355
[73] Chen J, Qin H J, Yang F, Liu J, Guan T, Qu F M, Zhang G H, Shi J R, Xie X C, Yang C L, Wu K H, Li Y Q and Lu L 2010 *Phys. Rev. Lett.* **105** 176602
[74] Liu M, Zhang J, Chang C Z, Zhang Z, Feng X, Li K, He K, Wang L L, Chen X, Dai X, Fang Z, Xue Q K, Ma X and Wang Y 2012 *Phys. Rev. Lett.* **108** 036805
[75] Yong S K, Brahlek M, Bansal N, Edrey E, Kapilevich G A, Iida K, Tanimura M, Horibe Y, Cheong S W and Oh S 2011 *Phys. Rev. B* **84** 073109
[76] Brahlek M, Koirala N, Salehi M, Bansal N and Oh S 2014 *Phys. Rev. Lett.* **113** 026801
[77] Bansal N, Yong S K, Brahlek M, Edrey E and Oh S 2012 *Phys. Rev. Lett.* **109** 116804
[78] Lu H Z, Shi J and Shen S Q 2011 *Phys. Rev. Lett.* **107** 076801
[79] Liu M, Chang C Z, Zhang Z, Zhang Y, Wei R, He K, Wang L, Chen X, Jia J F, Zhang S C, Xue Q K, Ma X and Wang Y 2010 *Phys. Rev. B* **83** 165440
[80] Cha J J, Kong D, Hong S S, Analytis J G, Lai K and Cui Y 2012 *Nano Lett.* **12** 1107
[81] Lee J, Park J, Lee J H, Kim J S and Lee H J 2012 *Phys. Rev. B* **86** 245321
[82] Taskin A A, Sasaki S, Segawa K and Ando Y 2012 *Phys. Rev. Lett.* **109** 066803
[83] Steinberg H, Lalo J B, Fatemi V, Moodera J S and Jarilloherrero P 2011 *Phys. Rev. B* **84** 233101
[84] Li Z, Garate I, Pan J, Wan X, Chen T, Ning W, Zhang X, Song F, Meng Y, Hong X, Wang X, Pi L, Wang X, Wang B, Li S, Reed M A, Glazman L and Wang G 2015 *Phys. Rev. B* **91** 041401

[85] Sato T, Segawa K, Kosaka K, Souma S, Nakayama K, Eto K, Minami T, Ando Y and Takahashi T 2011 *Nat. Phys.* **7** 840

[86] Brahlek M, Bansal N, Koirala N, Xu S Y, Neupane M, Liu C, Hasan M Z and Oh S 2012 *Phys. Rev. Lett.* **109** 186403

[87] Xu S Y, Neupane M, Belopolski I, Liu C, Alidoust N, Bian G, Jia S, Landolt G, Slomski B, Dil J H, Shibayev P P, Basak S, Chang T R, Jeng H T, Cava R J, Lin H Bansil A and Hasan M Z 2015 *Nat. Commun.* **6** 6870

[88] Lou R, Liu Z, Jin W, Wang H, Han Z, Liu K, Wang X, Qian T, Kushnirenko Y, Cheong S W, Osgood R M, Ding H and Wang S 2015 *Phys. Rev. B* **92** 115150

[89] Salehi M, Shapourian H, Koirala N, Brahlek M J, Moon J and Oh S 2016 *Nano Lett.* **16** 5528

[90] Wu L, Brahlek M, Aguilar R V, Stier A V, Morris C M, Lubashevsky Y, Bilbro L S, Bansal N, Oh S and Armitage N P 2013 *Nat. Phys.* **9** 410

[91] Sim S, Koirala N, Brahlek M, Ji H S, Park J, Cha S, Jo M H, Oh S and Choi H 2015 *Phys. Rev. B* **91** 235438

[92] Linder J, Yokoyama T and Sudbø A 2009 *Phys. Rev. B* **80** 205401

[93] Zhang M, Wang H, Mu K, Wang P, Niu W, Zhang S, Xiao G, Chen Y, Tong T, Fu D, Wang X, Zhang H, Song F, Miao F, Sun Z, Xia Z, Wang X, Xu Y, Wang B, Xing D and Zhang R 2018 *ACS Nano* **12** 1537

[94] Yang J, Zhang X and Miao R D 2014 *Acta Phys. Sin.* **63** 217202 (in Chinese)

[95] Fan Y, Upadhyaya P, Kou X, Lang M, Takei S, Wang Z, Tang J, He L, Chang L T, Montazeri M, Yu G, Jiang W, Nie T, Schwartz R N, Tserkovnyak Y and Wang K 2014 *Nat. Mater.* **13** 699

[96] Fan Y, Kou X, Upadhyaya P, Shao Q, Pan L, Lang M, Che X, Tang J, Montazeri M, Murata K, Chang L T, Akyol M, Yu G, Nie T, Wong K, Lou J, Wang Y, Tserkovnyak Y and Wang K 2016 *Nat. Nanotech.* **11** 352

[97] Mellnik A R, Lee J S, Richardella A, Grab J L, Mintun P J, Fischer M H, Vaezi A, Manchon A, Kim E A, Samarth N and Ralph D C 2014 *Nature* **511** 449

[98] Wang Y, Deorani P, Banerjee K, Koirala N, Brahlek M, Oh S and Yang H 2015 *Phys. Rev. Lett.* **114** 257202

[99] Shiomi Y, Nomura K, Kajiwara Y, Eto K, Novak M, Segawa K, Ando Y and Saitoh E 2014 *Phys. Rev. Lett.* **113** 196601

[100] Deorani P, Son J, Banerjee K, Koirala N, Brahlek M, Oh S and Yang H 2014 *Phys. Rev. B* **90** 094403

[101] Jamali M, Lee J S, Jeong J S, Mahfouzi F, Lv Y, Zhao Z, Nikolić B K, Mkhoyan K A, Samarth N and Wang J P 2015 *Nano Lett.* **15** 7126

[102] Baker A A, Figueroa A I, Collinsmcintyre L J, Laan G V D and Hesjedal T 2015 *Sci. Rep.* **5** 7907